MAGNETIC RESONANCE IN MEDICINE **28,** 275–289 (1992)

Projection Reconstruction Techniques for Reduction of Motion Effects in MRI

G. H. GLOVER* AND J. M. PAULY†

School of Medicine, Department of Diagnostic Radiology, and †Electrical Engineering Department, Stanford University, Stanford, California 94305-5105

Received March 25, 1992; revised May 12, 1992; accepted May 12, 1992

Projection reconstruction (PR) techniques are shown to have intrinsic advantages over spin–warp (2DFT) methods with respect to diminished artifacts from respiratory motion. The benefits result from (1) portrayal of artifacts as radial streaks, with the amplitude smallest near the moving elements; (2) streak deployment perpendicular to the direction of motion of moving elements and often residing outside the anatomic boundaries of the subject; (3) inherent signal averaging of low spatial frequencies from oversampling of central k-space data. In addition, respiratory-ordered view angle (ROVA) acquisition is found to diminish residual streaking significantly by reducing interview inconsistencies. Comparisons of 2DFT and PR acquisitions are made with and without ROVA. Reconstructions from magnitude-only projections are found to have increased streaks from motion-induced phase shifts.

INTRODUCTION

Since its introduction in the early 1980's, magnetic resonance imaging has received general acceptance as the method of choice for a substantial fraction of the neurological diagnostic imaging applications. This results from the superior contrast available with MRI, which allows a rich variety of contrast mechanisms to be exploited for a given diagnostic application. The success of MRI in neurological applications stems in part from the fact that the head may be readily immobilized even for relatively lengthy scans, which minimizes the possibility of ghosting artifacts caused by motion (*1*). This provides confidence that the full range of contrast manipulation methods may be invoked as necessary for neurological applications with minimal regard for the possibility of motion artifacts, which might otherwise limit the choice of sequence repetition time (TR), echo time (TE), and other parameters which affect contrast.

MRI applications in the abdomen have developed more slowly, on the other hand, because of the often severe artifacts induced by respiratory motion of the diaphragm, liver, and other organs (*2*). These artifacts appear as ghosts or smearing and are accompanied by blurring (*3*). The possibility of such artifacts lends an air of uncertainty in any given scan as to whether the resulting images will be diagnostic or not, and efforts to mitigate the ill effects may require alteration of scan protocols with possibly degraded contrast for cases when motion effects are particularly troublesome.

The origins of motion artifacts are well known by now. One source of artifact derives from intra-view motion either within the TE period or during the acquisition

0740-3194/92 $5.00

window itself. In these cases, motion-dependent phase shifts are developed from nonzero moments of the gradient waveforms used for spatial encoding or slice selection. The resulting image artifacts can be significant if the echo time is long (*4*) or for spins which are rapidly moving such as blood in major vessels (*5*).

The primary source of motion artifacts in abdominal imaging, however, is interview inconsistencies which result from altered disposition of the subject from one view to the next (*1*). The inconsistencies depend upon the details of the motion and can result in either amplitude or phase perturbations of the complex NMR signal. These perturbations in turn cause a modulation of the NMR data predominantly along the phase-encoding direction of k-space, which in turn is converted by the Fourier transform process into a displacement of the signal along that direction in the image. The result is streaks or ghosts from structures which have undergone motion during the scan, such as the abdominal wall or liver. The location of the misplaced signals depends on details of the motion relative to the acquisition timing and can be either well-focused as discrete ghosts when the motion is highly periodic or manifested as unstructured smearing of the moving components when the motion is aperiodic.

The nature of respiratory motion in the abdomen is a complex mixture of longitudinal and transverse translation and dilation of organs in response to the diaphragmatic cycle. Therefore, artifacts can arise from translation of tissue within the plane as well as with through-plane motion, as for example near the top of the liver in axial images. Often both types of motion occur simultaneously and can result in substantial blurring as well as ghosting since the motion components can be several centimeters in amplitude.

Many techniques have been developed and employed to reduce respiratory motion artifacts. These include gradient moment nulling (*6–8*), spatial presaturation (*9*), averaging (*10*), respiratory-ordered phase encoding (*11, 12*), adaptive correction using navigator echoes (*3, 13*), and rapid imaging methods. With the exception of certain of the rapid scan methods, however, these techniques are all based upon alterations to spin–warp (2DFT) techniques. Failure of these "fixup" approaches therefore results in ghosting and blurring along the phase-encoding direction.

Rapid scan techniques implemented on conventional scanners (Turbo, GRASS (*14*), fast spin-echo (*15*), spiral scan (*16*), and echo planar (EPI) methods on special purpose systems (*17, 18*), acquire the images in a time short compared to physiological processes, thus providing perhaps the best respiratory "compensation" possible. While these methods are very promising, often the available contrast choices are compromised by the rapid acquisitions, which leave little time for relaxation weighting. These difficulties have been surmounted to some extent in Turbo sequences by the use of suitable preparatory pulses (*14, 19*), but the low SNR and/or spatial resolution of such "snapshot" or EPI methods often renders the images of marginal diagnostic value.

The present techniques for reduction of respiratory artifacts have widely divergent mechanisms but (with the exception of the spiral scan approaches and EPI) a common platform; namely, the use of 2DFT k-space trajectories for data acquisition. Thus, the manifestation of inter-view inconsistencies is common to all the methods, and their success is governed by the degree to which the inconsistencies from one Cartesian k_y line to the next can be mitigated. Little attention has been given to investigation of

the potential merits of other *k*-space trajectories themselves from the standpoint of intrinsic robustness to motion effects.

One application for which non-Cartesian trajectories have been found particularly effective is in imaging human lung parenchyma using projection reconstruction (PR) methods (*20*). Typical results show surprisingly small respiratory motion artifacts, as demonstrated in Fig. 1 in comparison with conventional spin–warp (2DFT) methods. The low artifact level is highly significant in lung applications because of low parenchymal proton density, strong susceptibility dephasing (*21, 22*), and substantial diffusion losses (*23*) encountered as a result of the intense local field gradients established by the aveolar structures. This results in weak lung signals which can therefore be overwhelmed by ghosting artifacts from the relatively intense chest wall fat. The significantly lower level of motion artifacts observed in PR lung imaging stimulated interest in the use of PR methods for more general imaging applications as a possible solution to motion effects.

Based on our initial observation of the apparently superior performance of projection reconstruction methods with respect to motion, a more extensive study of PR techniques was undertaken. A theory of the motion sensitivity of PR methods has been developed and experimentally verified. The effects of phase-sensitive reconstruction versus magnitude reconstruction, and respiratory-ordered view angulation (ROVA) have also been addressed.

While this work is aimed at the investigation of PR methods primarily for their intrinsic merit in reduction of motion artifacts, there are a number of additional aspects of radial *k*-space trajectories that are attractive. One such aspect is the potential for making the echo time extremely short, which has applications in imaging short T2 species (*24, 25*), elimination of T2 weighting, and reduction of flow artifacts in vessel imaging (*26*).

MOTION EFFECTS IN PR AND 2DFT

Fundamentally, the differences between the motion sensitivities of PR and 2DFT derive from the radial sampling in projection reconstruction methods compared with

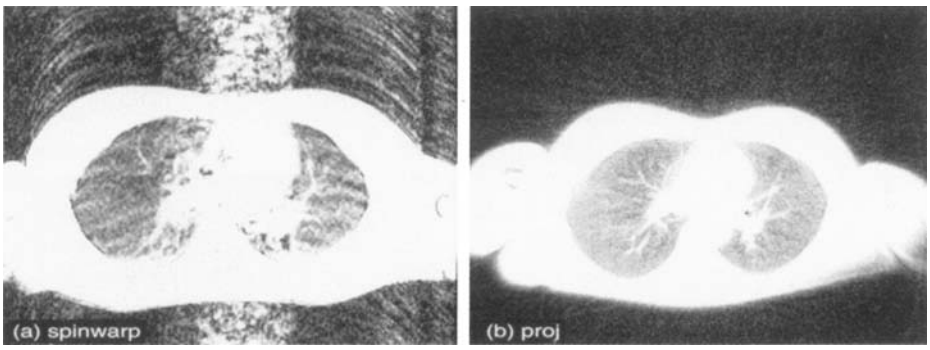

FIG. 1. Comparison of images obtained with (a) conventional T1-weighted multislice spin–warp: TR = 600 ms, TE = 20 ms, 256 × 4 NEX, scan time 8 min using respiratory compensation; and (b) multislice Hadamard projection reconstruction: TR = 200 ms, TE = 0.1 ms, 512 views × 8 NEX, scan time 4 min. The lack of motion artifacts with the PR sequence is critical to the successful visualization of lung parenchyma due to the low parenchymal signal.

the rectilinear k-space trajectories of 2DFT, as shown in Fig. 2. This leads to two effects with PR: (1) oversampling of the low spatial frequencies, which provides intrinsic averaging of the gross features of the subject, and (2) the generation of artifacts as streaks emanating from the moving structure and perpendicular to the direction of motion rather than as ghosts displaced along one (phase-encoding) direction.

The first basic difference between 2DFT (spin–warp) and PR trajectories is that the former samples k-space with uniform density whereas the latter oversamples the low spatial frequencies with $1/|k|$ redundancy. The choice of sampling strategy will influence the noise spectral density, and therefore contrast-detail characteristics. It is sometimes argued that oversampling the center of k-space is preferred since the bulk of the object's energy is at low frequencies. This statement can be misleading since the diagnostic task often deals with detecting and characterizing lesions, not detecting the entire object. For imaging a small lesion, uniform sampling is ideal since such an object has uniform energy throughout k-space (in the limit of a delta function). However, as the size of the target structure increases, sampling densities that emphasize low frequencies are preferred. This latter scenario is most prevalent in cancer imaging since typical lesions are many pixels in size, in which case PR imaging with its enhanced sampling density at low frequencies should outperform 2DFT imaging.

The comparison between PR and 2DFT is even more favorable when effects of motion are considered. In particular, T2-weighted images are often corrupted from motion-induced phase shifts that accrue during the long TE period. These phase shifts arise from bulk motion of entire organs whose spectrum therefore contains mostly low spatial frequencies. Even in short-TE sequences, inter-view amplitude perturbations may result from through-plane motion of organs. In either case, with 2DFT methods these perturbations result in a broad dispersion of signal in the phase-encoded direction. With PR, however, the oversampling of low frequencies will behave exactly as signal averaging since the artifacts arise from errors at low spatial frequencies. It is expected,

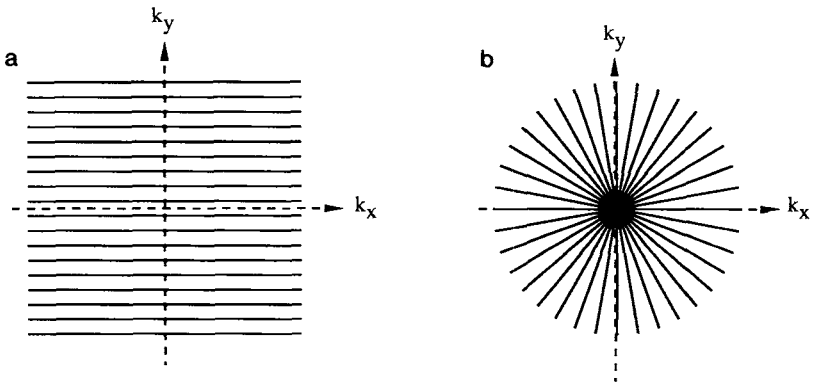

FIG. 2. The k-space trajectories for (a) spin–warp imaging and (b) projection reconstruction methods. Note that the low-frequency components are sampled for *every view* in PR, which provides intrinsic signal averaging for those components responsible for the gross features and contrast in the image, with artifact reduction benefits similar to those of conventional signal averaging. In 2DFT, each spatial frequency component is sampled uniformly and only once.

therefore, that motion artifacts in PR images will be greatly diminished compared to 2DFT.

The second fundamental difference between 2DFT and PR methods is the manner in which motion-generated inconsistencies create artifacts in the image. In 2DFT techniques each line in k-space (view) is typically acquired in <10 ms, while the delay between views (TR) is much longer. Motion inconsistencies thus propagate in the phase-encoding direction as displaced signal and blurring. With PR methods, inter-view inconsistencies cause streaks to emanate tangentially from the moving objects, which therefore can spread the artifact energy in all directions rather than just one. This tends to reduce the intensity of individual streaks. Moreover, because the streaks occur predominantly perpendicular to the direction of motion, they often reside outside the subject, especially those emanating from the relatively intense anterior wall fat. The radial character also propitiously alters the streak intensity as a function of distance from the source. This aspect is discussed next with a theoretical development of motion effects in 2DFT and PR acquisitions.

Theory: Periodic Motion

Consider a single point object which undergoes sinusoidal translation on the y axis with average location at the origin. Because of the linearity of the reconstruction process (either PR or 2DFT), more complex motion can be modeled by superposition. Location of the point at the origin simplifies the analysis but does not result in loss of generality. Let the intensity of the point be normalized to unity. Then, the projection of the object at view angle θ is

$$p_\theta(r) = \delta[r - a_0\cos(\theta)\sin(\Omega\theta/2\pi)], \qquad [1]$$

where a_0 and Ω represent the amplitude and frequency in cycles per scan, respectively, of the motion, and r measures location along the projection. The PR image is given by (27) (ignoring an intensity scaling factor)

$$f_{\mathrm{PR}}(\rho, \phi) = \int_0^{2\pi}\int_0^{k_m} e^{ik\rho\cos(\phi-\theta)}P_\theta(k)kdkd\theta, \qquad [2]$$

where $P_\theta(k) = F(p_\theta(r)) = e^{ia_0k\cos(\theta)\sin(\Omega\theta/2\pi)}$, F denotes Fourier transformation, and k_m is a maximum spatial frequency defined by sampling considerations. One finds, using a series expansion for the exponential,

$$f_{\mathrm{PR}}(\rho, \phi) = \sum_{m,l=-\infty}^{\infty} i^{(m+l)\Omega}e^{-in\phi}\int J_n(\rho k)J_m(a_0k/2)J_l(a_0k/2)kdk, \qquad [3]$$

with $n = m(\Omega - 1) + l(\Omega + 1)$. Inspection of [3] shows that the integrand is negligible if the radius ρ is small because the Bessel function $J_n(x) \sim 0$ unless the argument is comparable to the order. Thus, away from the origin the image will contain streaks with an azimuthal period determined by Ω, but *which have little energy close to the object itself* (ρ *small*). The radius at which the streaks become appreciable depends on the motion frequency, Ω. This is demonstrated in the simulations, below.

For a 2DFT sequence in which the phase-encoding order is sequential in time, the moving point generates a signal described by $P(k_x, k_y) = e^{-ia_0k_y\sin(\Omega k_yD)}$ using the same notation as above and with a field of view D. The reconstruction is given by

$$f_{2DFT}(x, y) = \delta(x) \sum_n q_n(y - n\Omega D), \quad [4]$$

where

$$q_n(y) \equiv i^n \int J_n(a_0 k_y) e^{ik_y y} dk_y. \quad [5]$$

The term with $n = 0$ in [4] represents the object at its true location, while the other terms describe ghost images of the point at distances which depend on the frequency of the motion. The amplitude of the higher order terms decreases with increasing n because of the spectral characteristics of the Bessel functions. Therefore, the maximum intensity of the artifacts occurs for the lowest order ghosts, i.e., *those ghosts closest to the object* (excluding aliasing wrap-arounds).

Reconstruction simulations of both PR and 2DFT methods were performed for an object centered at the origin having a Gaussian intensity profile. The results are shown in Fig. 3. As may be seen with 2DFT acquisition (Figs. 3e and 3f), the moving object creates ghosting artifacts which are strongest close to the object and which can overlap useful regions of larger objects. On the other hand, the PR method produces radial streaks which emanate from the object, but whose intensity close to the object is negligible (Figs. 3b and 3c). As predicted by [3], the frequency of the motion determines the radius at which the streaks become visible, with higher frequencies increasing

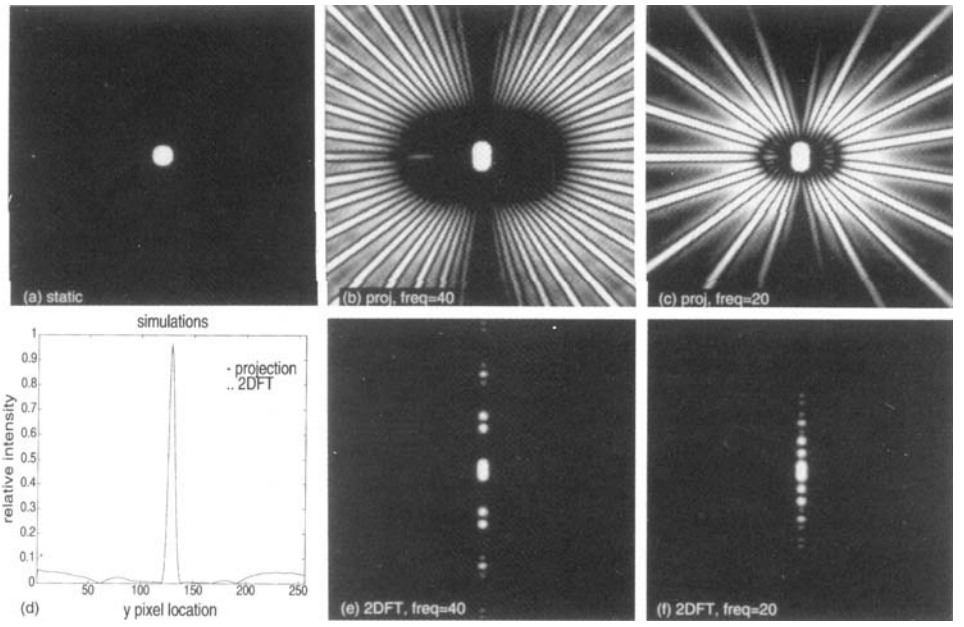

FIG. 3. Simulation results for sinusoidal vertical motion about origin of single object, Gaussian profile. (a–c) Streaks in PR are conspicuous at a frequency-dependent radius. (d) Plot of intensity through $y = 0$ of (b) and $x = 0$ of (e), showing relative magnitude of artifacts. (e, f) The 2DFT results show ghosts brightest close to the object's true location.

the artifact-free zone. Although in these simulations the object was located at the isocenter of projection space for convenience, the streak intensity is not related to radius from the origin, but rather depends on distance from the source object, wherever it may be.

Thus, the character of the PR artifacts for periodic motion is such that they occur at a distance from the moving structure, which is quite different from the case with Cartesian sampling. In addition, they are most apparent in directions perpendicular to the motion, instead of being arrayed wholly along the phase-encoding direction as evidenced by the asymmetry in Fig. 3b. There is a strong parallel to view aliasing artifacts (*28*), which derive from insufficient number of views and which occur only outside a certain radius.

Theory: Impulsive Motion

Consider now a symmetric object $o(r)$ located at the origin, which is displaced impulsively along the y axis just once during the scan, at view angle θ_0. Specifically, let the projections of the object be

$$p_\theta(r) = \begin{cases} p^0(r - a_0\cos\theta_0), & \theta = \theta_0 \\ p^0(r), & \text{elsewhere.} \end{cases} \quad [6]$$

Then, the Fourier transform of the *error* in the projection data is given by

$$\Delta P_\theta(k) = \begin{cases} (e^{-ika_0\cos\theta_0} - 1)P^0(k), & \theta = \theta_0 \\ 0, & \text{elsewhere,} \end{cases} \quad [7]$$

where $P^0(k) = F(p^0)$, so that the PR artifact is given by

$$\Delta f_{PR}(\rho, \phi) = \int_0^{k_m} e^{ik\rho\sin(\phi-\theta_0)}(e^{-ika_0\cos\theta_0} - 1)P^0(k)kdk. \quad [8]$$

Let $\xi = r\sin(\phi - \theta_0)$, which measures distance from the origin perpendicular to the projection direction, θ_0. Then

$$\Delta f_{PR}(\xi) = (-S(\xi) + S(\xi - a_0\cos\theta_0))/N_v, \quad [9]$$

where N_v is the number of views, and

$$S(\xi) = \int_0^{k_m} P^0(k)ke^{ik\xi}dk. \quad [10]$$

Thus, the artifact propagates along a direction parallel to view direction θ_0 at which the displacement occurred and is strongest when that direction is perpendicular to the direction of motion (in this case on the y axis with $\theta_0 = 0$ or π). This is depicted in Fig. 4a with plots of the normalized artifact intensity as a function of the angle between the motion and displacement view angle $(\pi/2 - \theta_0)$ for an object with $p^0(r) = \exp(-r^2/w^2)$, $w = 5$ pixels in a field of view $N = 256$. As shown in Fig. 4b and Eq. [9], there are in reality two streaks: a negative one at the location where the object would have been if it had been static, and a positive streak from its position during the impulsive displacement. Note that motion along the projection direction causes no artifact (θ_0

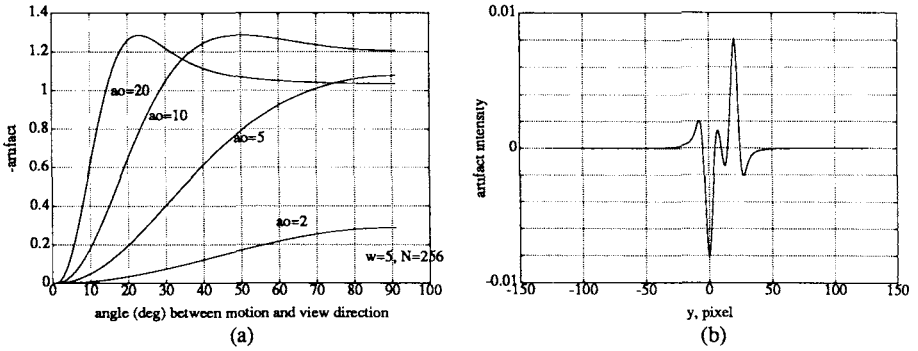

FIG. 4. Artifact for impulsive motion in PR. (a) Artifact intensity at origin, normalized to intensity for $a_0 = \infty$. For small-amplitude motion, streak intensity is small unless θ_0 is perpendicular to motion direction (0). (b) Plot of artifact intensity on y axis, normalized to signal at the origin for $a_0 = 20$. Two streaks occur; interference between them accounts for values greater than unity in (a).

$= \pi/2$ or $3\pi/2$ in this example with vertical motion). By extrapolation to scanning humans, therefore, motion of the abdominal wall can be expected to cause artifacts tangential to the wall, which will therefore be largely outside of the subject and less troublesome than if, as in 2DFT, the same amount of misplaced signal is projected as ghosts in one direction, which can overlap the structures of interest.

Impulsive motion during 2DFT scanning causes streaking along the phase-encoding direction in the image, with character which depends on the spatial frequency being collected when the impulsive displacement occurred. If this frequency is denoted by k_y and the displacement is along the y axis with an amplitude a_0 as for the PR example, the artifact is given by

$$\Delta f_{2DFT}(y) = P^0(k_y)(e^{ik_y a_0} - 1)e^{ik_y y}/N_v\delta(x), \quad [11]$$

which has magnitude

$$|\Delta f_{2DFT}(y)| = P^0(k_y)\sin(k_y a_0/2)(2/N_v)\delta(x). \quad [12]$$

In contrast to PR, the artifact propagates in the vertical (phase-encoding) direction as a smear with amplitude cyclically dependent on k_y and a_0. Motion in the x direction would have produced an artifact with additional horizontal extent, but the smear would still have propagated in the y direction.

PROJECTION RECONSTRUCTION METHOD: *IN VIVO* RESULTS

A multislice pulse sequence was developed for full-echo PR scanning as shown in Fig. 5b. This sequence is employed for conventional TE choices; also shown (Fig. 5a) is a sequence which has been described previously for TEs as short as 100 μs (*25*), using FID acquisition with a one-half k-space RF excitation pulse. In the full echo acquisitions, an odd number of views covering 360° was used to eliminate twofold redundancy in k-space coverage. A 16-ms sinc pulse was employed to diminish the fat signal by saturating the lipid spins. These sequences were implemented on a com-

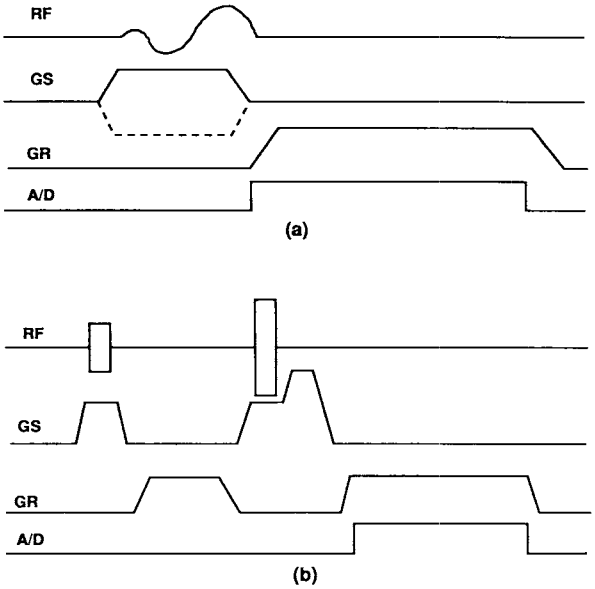

FIG. 5. Pulse sequences for PR spin-echo imaging. (a) Short-TE sequence uses a one-half pulse to allow slice selection with minimal echo delay. (b) Spin-echo sequence for collection of k-space diameters.

mercial 1.5-T whole-body scanner employing shielded gradients (GE Signa, Rev. 4.7, Milwaukee, WI).

Reconstructions were performed on an external workstation (Sun Microsystems, Mountain View, CA) using a gridding algorithm (*29*) to reformat the radial k-space data into Cartesian format for 2D Fourier transformation. The gridding method uses convolution of the data with a 2D kernel whose width increases with radius, k. The output grid is oversampled by a factor of 2 to eliminate sampling aliasing and to diminish the intensity roll-off due to the gridding filter. This algorithm was used instead of the more conventional filtered backprojection because of its flexibility for accommodating short-TE acquisitions with FIDs, which require resampling of the data to correct for nonconstant k-space velocity during gradient ramp-up. It has no particular advantages for motion reduction, however.

Scans of abdominal sections were performed on normal volunteers using multislice PR and conventional 2DFT spin–warp methods. Representative images are shown in Fig. 6. Artifacts in the conventional scans are portrayed as ghosts within the liver and as general smearing of energy in the vertical (phase-encoding) direction. By contrast, the PR scans show no structured ghosts within the confines of the subject, although some streaks are evident tangential to the abdominal wall as expected from the simulations and CT experience, and some residual streaks arise within the subject. No motion compensation was employed for either set of scans.

A potential problem with PR techniques is that local off-resonance conditions resulting from B_0 heterogeneity or chemical shift produce signal loss and blurring, as may be seen within the subcutaneous fat. The effect of off-resonance is demonstrated

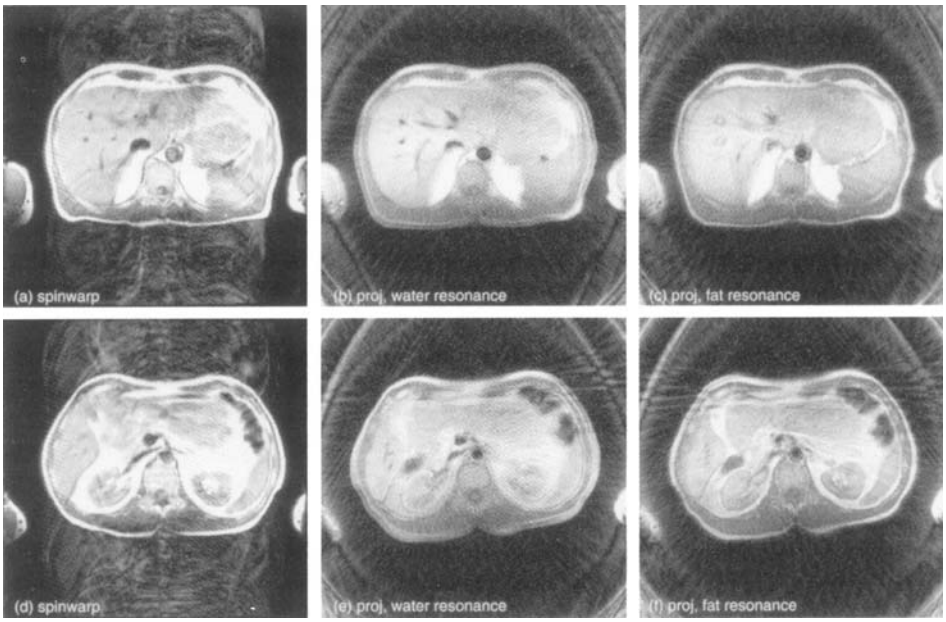

FIG. 6. Two slices of volunteer comparing 2DFT (spin–warp) and PR. TE = 20 ms, TR = 400 ms, same scan time. (a, d) 2DFT, 256 × 2 NEX. (b, e) PR, 511 views × 1 NEX. Streaks from abdominal fat are less intense in PR and lie primarily outside the body. (c, f) Same PR data, reconstructed with fat on resonance. Off resonance causes blurring (compare anterior fat and hepatic vessels in (b) and (c)).

in Figs. 6c and 6f by introducing an offset of 3.2 ppm into the reconstruction, appropriate to placing the fat on resonance. Note that while the fat components are now in focus, the water structures are blurred (e.g., hepatic vessels). Thus, a regional correction for unavoidable off-resonance conditions from chemical shift or B_0 heterogeneity may be necessary for general applicability of PR in abdominal scanning. A chemical-shift selective rf saturation pulse (*30*) was employed in an attempt to suppress the signal from the fat. Its poor suppression is the result of B_0 and B_1 heterogeneity and confirms that a more effective method for fat suppression or correction is needed. Fat saturation was not employed in the spin–warp images, but its use might have reduced the abdominal wall ghosts subject to the same limitations in the degree of suppression.

RESPIRATORY ORDERED VIEW ANGULATION

As depicted in Fig. 6 and described above theoretically, PR methods have certain intrinsic advantages over 2DFT techniques with respect to motion sensitivity. Nevertheless, residual streaks are generated by interview inconsistencies, and they may be detrimental to diagnostic image quality. Accordingly, a respiratory compensation technique conventionally used with 2DFT methods called EXORCIST (*12*) was adapted for use with the PR technique.

In 2DFT EXORCIST, the phase-encoding order for the N_v views is chosen dynamically during the scan using a respiration monitor in such a way that the apparent

motion frequency is made either as slow as possible (1 respiratory cycle/scan) or as high as possible ($N_v/2$ cycles per scan). This causes the ghosts to be either as close to the moving object as possible for the first ("low-sort") case (1 pixel away) or as far away as possible for the second ("high-sort") case (one-half the image field of view). Experience has shown that the artifacts are minimized when the subject's respiration state is made as smooth as possible between adjacent views (in the low-sort case).

For PR therefore, a monotonic sort algorithm was employed to map the view angle uniformly to respiratory phase in order to minimize adjacent view motion. This algorithm, respiratory ordered view angulation, uses the scanner's conventional respiration monitoring pneumatic bellows and firmware for real-time choice of view angle according to the preprogrammed view sort pattern. No additional scan time was thereby incurred.

Typical results are illustrated in Fig. 7. Sinograms obtained with ROVA show significant reductions in view-to-view variations caused by breathing, compared with the scan without ROVA. The smoother variations in the raw data are reflected in diminished streak artifacts as well as reduced blurring in the images (compare Figs. 7c and 7d). The reduced blurring, not obtained with such methods applied in conventional 2DFT, is again a consequence of radial k-space sampling and thus represents a clear advantage for PR. Other sort patterns may be even more beneficial as discussed below.

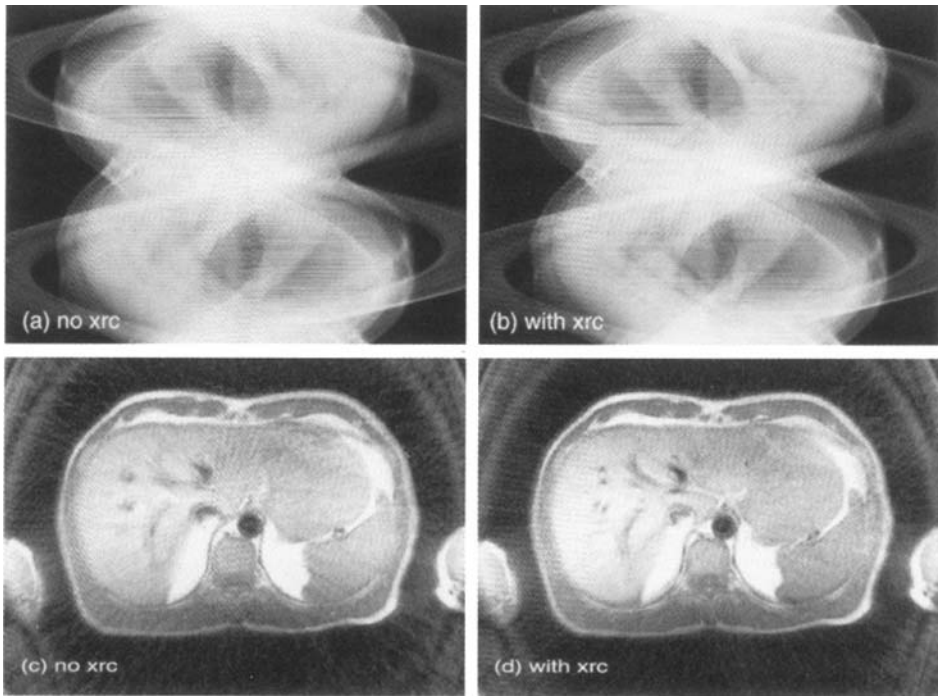

FIG. 7. Sinograms without (a) and with (b) respiratory-ordered view angulation; corresponding images in (c) and (d). ROVA reduces interview respiratory motion.

Many of the remaining streaks in Fig. 7 result from pulsatile motion of the vessel walls which cause inconsistencies. However, most of these artifacts derive from the residual flowing blood signal in the aorta and vena cava, a result of the relatively short TE and lack of spatial presaturation. Gradient moment nulling could also be used to diminish the artifacts, although the increased conspicuity of the blood may be detrimental in some applications.

MAGNITUDE VERSUS PHASED RECONSTRUCTION

Respiratory motion causes both amplitude and phase inconsistencies from view to view. It was found that flow artifacts in PR acquisitions were diminished when the phase of the projections was discarded before back-projection (*31*). Therefore, the role of phase in PR reconstruction was examined with respect to respiratory motion.

The algorithm utilized for this investigation employed three steps. Let $P_\theta(k)$ be the collected projection data for a view at angle θ. Then a magnitude projection set is obtained from these data as

$$P_\theta^m(k) = \mathcal{F}^{-1}\{|\mathcal{F}(P_\theta(k))|\}. \quad [13]$$

This algorithm was applied to the ROVA data used in Fig. 7 to generate a new magnitude-only set of data, which was then reconstructed as usual. Results are shown in Fig. 8, where it may be seen that the magnitude-only reconstruction has greater streaking than the phased reconstruction. This shows that a major fraction of typical motion artifacts in PR derive from phase accumulation, and that ignoring phase causes greater inconsistencies from view to view. Thus it is important to retain the phase information for motion robustness.

DISCUSSION

Projection reconstruction methods depict inconsistencies from motion (in-plane and through-plane) quite differently than spin–warp techniques. Because the resulting streaks tend to be arrayed tangentially to moving structures and may not be conspicuous until some distance from the source, the artifacts are often not as detracting as in

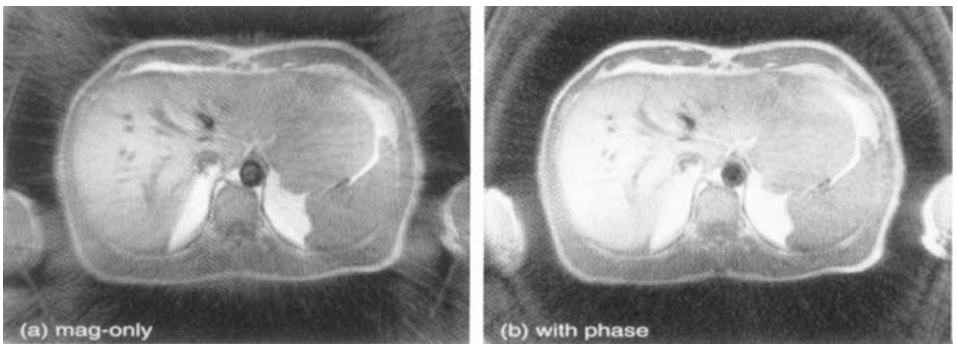

FIG. 8. Comparison of magnitude-only (a) versus conventional reconstructions. Additional streaks in (b) result from motion-induced phase shifts.

2DFT, where the ghosts are exhibited in one direction only, have strongest intensities closest to the source, and may occur at any distance. These results were suggested by the simulations of moving point objects and were confirmed by scans of abdominal sections.

In many applications such as imaging of the kidneys, pancreas, or adrenals, the organs are relatively static, but the images are nevertheless degraded by severe ghost replications or smearing from other moving structures such as abdominal wall fat. In this case local motional blurring is not the dominant cause of the image degradation. Therefore PR methods can play a very strong role here, because even without algorithmic corrections the intrinsic lack of ghost artifacts with these methods can provide superior anatomic depiction free of local blurring.

The use of ROVA for prospective choice of view angle consistent with minimal inter-view irregularity has been shown to significantly reduce residual streak artifacts. Alternatives to the low-sort pattern employed in this paper may provide additional benefit. It has been found, for example, that while the peak-inspiration state is irregular even for highly motivated volunteers, the end-expiration state is usually quite uniform and reproducible over extended time periods. Thus a better sort strategy may be to allocate views which are horizontal ($\theta \sim 0$ or π) to end-expiration, while using peak-inspiration periods for vertical views (θ near $\pi/2$ and $3\pi/2$). This strategy causes views which are most sensitive to vertical motion (e.g., of the anterior wall) to be acquired during maximum uniformity of the respiratory cycle and relegates views acquired during irregular respiration states to verticals views for which vertical motion is of little consequence.

Phase information contained in the projections has been shown to be a significant contributor to residual motion streaks in PR. A simple illustration demonstrates the plausibility of this. Consider a square object split exactly in half horizontally, for which the signal in the bottom half is the negative of that in the top. A phased projection taken along a vertical direction will be nil, while a horizontal projection will be nonzero and bipolar. Phase-sensitive reconstruction from these projections will be perfectly consistent, while a magnitude-only projection reconstruction will have gross inconsistencies from the unipolar horizontal projection compared with the null vertical one. Thus it can be expected that the phase information is important since the NMR projections are made from vectorial summations.

In some applications for which the echo time must be kept short, as in imaging lung (Fig. 1) or in fibrotic atherosclerotic plaque (*32*), PR offers the only method that can provide ultrashort TE. In such cases the acquisition begins during the rising edge of the projection gradient (Fig. 5a), which requires correction during reconstruction for the nonuniform sampling velocity in k-space. However, this provides additional low-frequency redundancy over full-echo PR, which may have further advantages in artifact suppression.

The choice of 360° coverage for the view sampling was made in order to use angular interleaving with an odd number of views and to provide a symmetric point response function for off-resonance-induced blurring. Alternatively, 180° could be covered with the same number of views (if needed for SNR purposes) using averaging. If the additional SNR were not needed, this would allow a reduction in scan time, and perhaps motion artifacts as well. An additional benefit of the angular interleaving, which causes

views collected temporally far apart to be juxtaposed in projection angle, is that it minimizes the discontinuity between the views at 0° and 360°. Such discontinuities often cause artifacts in CT scanning. In the scans reported here, an extra view was collected at 360°, which is redundant with the view at 0° in the absence of motion. No significant benefit was derived from averaging the two views together, suggesting that the requirement of rotational periodicity was adequately fulfilled or blurred by the interleaving.

PR methods were found to be more sensitive to off-resonance conditions that derive from chemical shifts or local B_0 heterogeneity. Our preliminary results suggest that fat suppression by selective saturation is not robust in diminishing the signal from fat and that a more effective lipid suppression technique such as selective excitation or a regional blurring correction (*33*) may be needed.

A second potential disadvantage of PR techniques is that inconsistencies from flowing blood result in radial streaks which can be significant. However, spatial presaturation of the in-flowing spins can be employed to reduce the intensity. Alternatively, gradient moment nulling can be used to reduce the velocity sensitivity of the acquisitions, thereby also reducing the streaking.

Overall, projection reconstruction methods appear to have intrinsic advantages over 2DFT k-space trajectories from the standpoint of motion robustness. This results from the distribution of artifacts in PR predominantly as streaks perpendicular to the direction of motion, rather than as ghosts, and with intensities which are often weaker near the source of the motion. This provides an effective platform for augmentation by prospective, adaptive view-ordering to provide abdominal scans with diminished motion effects. Other techniques utilize consistency criteria derived from the central slice theorem to exclude projection components which result from motion of the object. These techniques are currently under investigation and will be reported elsewhere.

REFERENCES

1. V. J. WEDEEN, R. E. WENDT, AND H. M. JEROSCH, *Magn. Reson. Med.* **11,** 114 (1989).
2. L. AXEL, R. M. SUMMERS, H. Y. KRESSEL, AND C. CHARLES, *Radiology* **160,** 795 (1986).
3. R. L. EHMAN AND J. P. FELMLEE, *Radiology* **173,** 255 (1989).
4. P. SCHMALBROCK, C. YUAN, D. W. CHAKERES, J. KOHLI, AND N. J. PELC, *Radiology* **175,** 861 (1990).
5. J. LISTERUD, *Magn. Reson. Quarterly* **7,** 136 (1991).
6. J. D. LIPCAMON, L. C. CHIU, J. J. PHILLIPS, AND P. M. PATTANY, *Radiol. Technol.* **59,** 415 (1988).
7. P. M. PATTANY, J. J. PHILLIPS, L. C. CHIU, J. D. LIPCAMON, J. L. DUERK, J. M. MCNALLY, AND S. N. MOHAPATRA, *J. Comput. Assist. Tomogr.* **11,** 369 (1987).
8. J. G. PIPE AND T. L. CHENEVERT, *Magn. Reson. Med.* **19,** 175 (1991).
9. J. P. FELMLEE AND R. L. EHMAN, *Radiology* **164,** 559 (1987).
10. M. L. WOOD AND R. M. HENKELMAN, *Med. Phys.* **13,** 794 (1986).
11. D. R. BAILES, D. J. GILDERDALE, G. M. BYDDER, A. G. COLLINS, AND D. N. FIRMIN, *in* "Proceedings, Fourth Annual Meeting, Society of Magnetic Resonance in Medicine, 1985," p. 939.
12. G. GLOVER AND N. PELC, Method of reducing image artifacts due to periodic signal variances in NMR imaging, U.S. Patent No. 4,663,591, 1988.
13. J. J. E. CUPPEN, J. P. GROEN, J. J. E. IN DEN KLEEF, AND H. A. TUITHOF, *in* "Proceedings, Fourth Annual Meeting, Society of Magnetic Resonance in Medicine, 1985, p. 962.
14. A. HAASE, *Magn. Reson. Med.* **13,** 77 (1990).
15. P. S. MELKI, R. V. MULKERN, L. P. PANYCH, AND F. A. JOLESZ, *J. Magn. Reson. Imaging* **1,** 319 (1991).

16. C. H. MEYER AND A. MACOVSKI, *in* "Proceedings, Sixth Annual Meeting, Society of Magnetic Resonance in Medicine, 1987, p. 230.
17. P. MANSFIELD AND A. A. MAUDSLEY, *J. Magn. Reson.* **27,** 129 (1977).
18. R. J. ORDIDGE, R. COXON, A. HOWSEMAN, B. CHAPMAN, R. TURNER, M. STEHLING, AND P. MANSFIELD, *Magn. Reson. Med.* **8,** 110 (1988).
19. R. A. JONES AND T. E. SOUTHON, *Magn. Reson. Med.* **19,** 483 (1991).
20. C. J. BERGIN, J. M. PAULY, AND A. MACOVSKI, *Radiology* **179,** 777 (1991).
21. C. J. BERGIN, G. H. GLOVER, AND J. M. PAULY, *Radiology* **180,** 845 (1991).
22. C. J. BERGIN, D. C. NOLL, J. M. PAULY, AND A. MACOVSKI, *Radiology* **181(P),** 117 (1991).
23. G. H. GLOVER, J. M. PAULY, AND C. J. BERGIN, *Radiology* **181(P),** 280 (1991).
24. J. B. RA, S. K. HILAL, AND Z. H. CHO, *Magn. Reson. Med.* **3,** 296 (1986).
25. J. M. PAULY, S. CONOLLY, D. NISHIMURA, AND A. MACOVSKI, *in* "Proceedings, Eighth Annual Meeting, Society of Magnetic Resonance in Medicine, 1989, p. 28.
26. D. G. NISHIMURA, A. MACOVSKI, J. I. JACKSON, R. S. HU, C. A. STEVICK, AND L. AXEL, *Magn. Reson. Med.* **8,** 96 (1988).
27. G. H. GLOVER AND R. L. EISNER, *J. Comput. Assist. Tomogr.* **3,** 85 (1979).
28. P. M. JOSEPH AND R. A. SCHULTZ, *Med. Phys.* **7,** 692 (1980).
29. J. I. JACKSON, C. H. MEYER, D. G. NISHIMURA, AND A. MACOVSKI, *IEEE Trans. Med. Imaging* **10,** 473 (1991).
30. P. M. JOSEPH AND A. SHETTY, *Magn. Reson. Imaging* **6,** 421 (1988).
31. K. J. JUNG AND Z. H. CHO, *Magn. Reson. Med.* **19,** 349 (1991).
32. G. E. GOLD, J. M. PAULY, G. H. GLOVER, J. C. MORETTO, A. MACOVSKI, AND R. J. HERFKENS, submitted for publication.
33. D. C. NOLL, Thesis, Stanford University, 1991.